

Freeze Extrusion Fabrication of 13-93 Bioactive Glass Scaffolds for Bone Repair

T.S. Huang,^{1*} N.D. Doiphode,² M.N. Rahaman,¹ M.C. Leu,² B.S. Bal,³ D.E. Day¹

¹Department of Materials Science and Engineering, and Center for Bone and Tissue Repair and Regeneration, Missouri University of Science and Technology, Rolla, Missouri 65409

²Department of Mechanical and Aerospace Engineering, Missouri University of Science and Technology, Rolla, Missouri 65409

³Department of Orthopaedic Surgery, University of Missouri–Columbia, Columbia, Missouri, 65212

Reviewed, accepted September 23, 2010

Abstract

There is an increasing demand for synthetic scaffolds with the requisite biocompatibility, internal architecture, and mechanical properties for the bone repair and regeneration. In this work, scaffolds of a silicate bioactive glass (13-93) were prepared by a freeze extrusion fabrication (FEF) method and evaluated *in vitro* for potential applications in bone repair and regeneration. The process parameters for FEF production of scaffolds with the requisite microstructural characteristics, as well as the mechanical and cell culture response of the scaffolds were evaluated. After binder burnout and sintering (60 min at 700°C), the scaffolds consisted of a dense glass network with interpenetrating pores (porosity \approx 50%; pore width = 100–500 μm). These scaffolds had a compressive strength of 140 ± 70 MPa, which is comparable to the strength of human cortical bone and far higher than the strengths of bioactive glass and ceramic scaffolds prepared by more conventional methods. The scaffolds also supported the proliferation of osteogenic MLO-A5 cells, indicating their biocompatibility. Potential application of these scaffolds in the repair and regeneration of load-bearing bones, such as segmental defects in long bones, is discussed.

Keywords: Freeze extrusion fabrication; bioactive glass; solid freeform fabrication; bone repair

*Corresponding author. E-mail: hts@mst.edu (T.S. Huang)

1. Introduction

There is an increasing demand for synthetic scaffolds with the requisite biocompatibility, mechanical properties and internal architecture for the repair and regeneration of tissues and organs. An ideal scaffold for bone repair and regeneration should have the following characteristics [1]: (1) biocompatible (non-toxic) with the ability to promote cell adhesion, proliferation, and differentiation; (2) porous three-dimensional (3D) architecture to allow cell proliferation, vascularization, and diffusion of nutrients between the cells seeded within the matrix and the surroundings; (3) mechanical properties comparable to the bone to be replaced; (4) ability to bond firmly to bone and soft tissue; (5) degradation rate similar to the rate at which new bone is formed; (6) processability into the desired anatomical shape.

Bioactive glass has several attractive properties for application as a scaffold material [2,3]. Bioactive glass reacts with the body fluids, forming a surface layer of hydroxyapatite (the main mineral constituent of bone) which is responsible for forming a firm bond with hard and soft tissues. Bioactive glass is osteoconductive as well as osteoinductive, and has a widely recognized ability to support new bone growth. However, porous bioactive glass scaffolds fabricated using conventional methods commonly have low strength (<20 MPa) [3,4], so their use in the repair and regeneration of load-bearing bones is challenging. Attempts are currently being made to improve the mechanical properties of bioactive glass scaffolds for the repair of load-bearing bones [4-6]. These attempts are focused mainly on the control of the pore shape, pore size, and pore orientation to improve the strength of the scaffolds.

Solid freeform fabrication (SFF) can potentially produce scaffolds with customized external shape, as well as predefined and reproducible internal architecture (porosity; pore size;

and pore distribution). An advantage of the SFF technology is the potential ease of creating scaffolds with the anatomical shape and dimensions tailored specifically to individual patients. SFF technologies involve building three-dimensional (3D) objects layer by layer. Although there are several variants of SFF technology, the general process involves producing a computer-generated model, which represents the physical prototype to be built, using computer-aided design (CAD) software. The model is next converted into a format that is analyzed by a computer, which slices the model into cross-sectional layers. The data is then implemented to the SFF machine which systematically produces the physical prototype layer by layer. Post-processing of the formed article is often necessary to remove temporary support structures or processing aids, particularly in the case of ceramic and glass particles that are commonly difficult to bond directly by most available SFF techniques.

The most widely researched SFF techniques include fused deposition modeling (FDM) of polymeric materials [7,8], fused deposition of ceramics (FDC) [9-11], selective laser sintering (SLS) [12,13], 3-D printing [14], stereolithography [15], and robocasting [16]. Freeze extrusion fabrication (FEF) has received less attention, but the technique has been used to fabricate dense ceramic articles for mechanical engineering applications [17]. FEF is based on a combination of techniques taken from fused deposition, freeze casting, and robocasting [18]. In FEF, an aqueous mixture with a paste-like consistency is extruded through an orifice to form filaments, which are frozen *in situ* to avoid slumping or distortion of the formed article. The rheology of the paste is critical for providing the plastic properties required for avoiding flaws in the formed article. After formation by FEF, the article is subjected to a freeze-drying step to sublime the frozen liquid.

In FEF of ceramic or glass, particles are commonly mixed with a polymeric binder phase to provide the required plastic properties for extrusion. FEF of these materials involve key post-processing steps. Following freeze drying to remove the frozen liquid, a binder removal step is necessary prior to a sintering step in which the particles are thermally bonded to form a strong network. Ideally, the binder phase used to impart the plasticity to the extrudate must be removed completely (typically by thermal decomposition) prior to the onset of the sintering step to avoid the presence of impurity phases in the final article. In the sintering step, the article is heated to a sufficiently high temperature to cause matter transport in order to bond the particles into a dense strong network. In the case of ceramics, the sintering temperature is typically 0.5–0.9 of the melting temperature, whereas the sintering temperature is typically between the glass transition temperature and the melting temperature for glass.

In the last decade, SFF methods have been widely applied to the production implants and scaffolds for biomedical applications. The biomaterials used in these studies have been mainly biodegradable polymers such as poly(glycolic acid), poly(lactic acid) and their copolymers, bio-inert metals such as titanium, and bioactive ceramics such as hydroxyapatite [19-28]. There is growing interest in the production of bioactive ceramics and bioactive glass scaffolds for potential bone repair applications because their attractive properties.

The objective of this work was to evaluate the feasibility of forming bioactive glass scaffolds using an FEF technique. The development of extrudable paste with optimized rheology and the process parameters for the production of scaffolds with pre-determined internal architecture were studied. A silicate bioactive glass designated 13-93 was used in this work because of our previous experience with forming scaffolds of this glass using more conventional

techniques. Products of 13-93 bioactive glass are also approved for *in vivo* use in the United States, Europe, and elsewhere [29].

2. Experimental Procedures

2.1. Preparation of starting materials and extrudable paste

The bioactive glass used in this work is designated 13-93, with the composition (wt%): 53.0 SiO₂, 6.0 Na₂O; 12.0 K₂O; 6.0 MgO, 20.0 CaO; 4.0 P₂O₅. Coarse particles of the glass were kindly provided by Mo-Sci Corp., Rolla, Missouri. The as-received glass particles were ground to a size finer than ~3 μm, using a combination of two methods. Particles of size smaller than 45 μm were first obtained by grinding the as-received particles in a steel shatterbox (SPEX SamplePrep LLC, Metuchen, NJ) and sieving the particles through a 325 mesh sieve. Approximately 100 g of these particles were then dispersed in deionized water and ground for 1 h in an attrition mill (Model 01-HD, Union Process, Akron, OH) using ZrO₂ grinding media. After evaporation of the water from the attrition-milled slurry using a hot plate, the particles were dried for 24 h in oven at 65°C. The dried, agglomerated powder was ground in an agate mortar and pestle, and sieved through a 325 mesh sieve.

An extrudable paste for use in the FEF process was prepared as follows. First, an aqueous-based slurry with the composition given in Table I, consisting of glass particles, deionized water, and polymeric additives, was formed into a homogeneous mixture by ball milling for 24 h using Al₂O₃ milling media. These polymeric additives were selected because they were used previously in the fabrication of Al₂O₃ articles by the FEF method [18]. Second, the ball-milled slurry was heated under a controlled temperature/time schedule (70 min at 65°C) to evaporate some of the water, and to control the viscosity of the paste. Pastes with different

viscosities were tested in the FEF equipment to determine whether they were extrudable, and the system with the optimum viscosity for extrusion was chosen by a trial-and-error method.

Table I. Composition of starting slurry used in the preparation of the extrudable paste for FEF.

Component	Concentration (vol%)	Function	Manufacturer
13-93 glass particles	40.00	Solid phase	Mo-Sci Corp., Rolla, MO
EasySperse	0.50	Dispersant	ISP Technologies, Inc., Wayne, NJ
Surfnol	0.50	Defoamer	Air Products & Chemicals, Inc., Allentown, PA
Glycerol	1.00	WCCA*	Alfa Aesar, Ward Hill, MA
PEG 400	1.00	Lubricant	Alfa Aesar, Ward Hill, MA
Aquazol 5	4.00	Binder	ISP Technologies, Inc., Wayne, NJ
Deionized water	53.00	Solvent	—

*WCCA: Water crystallization control agent

2.2 Freeze extrusion fabrication of bioactive glass scaffold

Figure 1 shows images of the main components of the FEF equipment used in this work. The paste to be extruded is loaded into a heated reservoir housed in a computer-controlled gantry that allows programmable movement in three dimensions. A nozzle attached to the reservoir determines the diameter of the extrudate which is deposited on a fixed platform cooled to the required temperature using liquid nitrogen. The system is contained within a cooled chamber.

In the present work, the fabrication environment temperature was -20°C . The paste was extruded layer by layer, with each layer deposited at 90° relative to the preceding layer. Based on the rheology of the paste, the software in the FEF machine was adjusted to control the extrusion force and rate of deposition. A nozzle diameter of $580\ \mu\text{m}$ was used in these experiments, and the spacing between adjacent filaments was $600\ \mu\text{m}$.

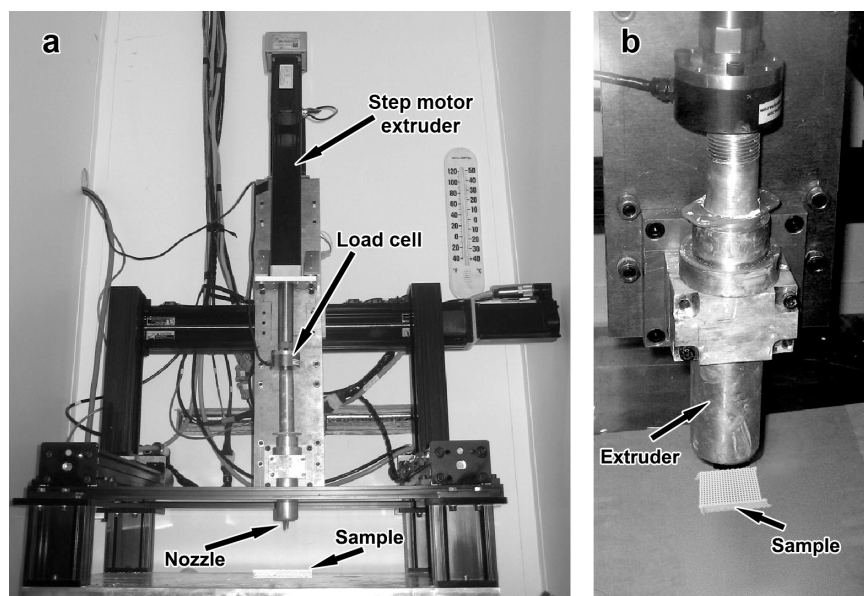


Figure 1. Images showing the main components of the freeze extrusion fabrication equipment used in the present work.

2.3. Post processing of as-formed FEF construct

The decomposition kinetics of the polymeric binder (without glass particles) were followed using thermogravimetric analysis (STA409, NETZSCH). Based on these kinetic data, a temperature–time schedule was developed for the removal of the polymeric additives from the as-formed FEF construct. The objective was to completely remove the binder by thermal decomposition prior to sintering of the glass particles. Incomplete removal of the binder prior to sintering resulted in scaffolds with a black color, due to residual carbon entrapped in the glass. A schedule lasting 5 days, consisting of a slow heating rate (3–5°C/h) and several isothermal holding stages, resulted in complete removal of the binder. Following the binder removal schedule, the construct was sintered in air for 1 h at 700°C (heating rate = 5°C/min) to densify the glass phase.

2.4. Structural and mechanical evaluation of 13-93 bioactive glass scaffolds

Following the sintering step, bioactive glass scaffolds were ground to form a powder (<45 μm) and analyzed using X-ray diffraction, XRD (Model D/mas 2550 v; Rigaku, The Woodlands, TX). The analysis was performed using Cu K_{α} radiation ($\lambda = 0.15406 \text{ nm}$) at a scanning rate of $0.01^{\circ} 2\theta/\text{min}$ in the range $3\text{--}90^{\circ} 2\theta$. The microstructure of the scaffold and the glass phase was examined using conventional methods in an optical microscope and a scanning electron microscope, SEM (S-4700; Hitachi, Japan).

The mechanical response of the fabricated scaffolds in compression was measured at a crosshead speed of 0.2 mm/min in an Instron machine (Model 4205; Instron, Norwood, MA). Six cube-shaped samples (5 mm in length), surface ground using a diamond coated wheel and sectioned using a diamond-coated blade from the fabricated scaffolds, were tested. The compression force was applied along the thickness direction of the scaffold.

2.5. Cell culture

The ability of the fabricated scaffolds to support the proliferation of MLO-A5 cells, an established murine osteogenic cell line, was used to confirm their biocompatibility. The MLO-A5 cells were kindly provided by Professor Lynda F. Bonewald, University of Missouri-Kansas City. After they were washed twice with water and dried, cube-shaped scaffolds (5 mm in length), similar to those used the mechanical tests described above, were sterilized by heating for 2 h at 500°C , seeded with $50,000$ MLO-A5 cells suspended in $100 \mu\text{l}$ of complete medium and incubated for 4 h to permit cell attachment. The cell-seeded scaffolds were then transferred to a 24-well plate containing 2 ml of complete medium per well. All cell cultures were maintained at 37°C in a humidified atmosphere of $5\% \text{ CO}_2$, with the medium changed every 2 days.

To visualize the metabolically active cells on and within the scaffolds, each cell-seeded scaffold was placed in 0.2 ml serum-free medium containing 0.1 mg of the tetrazolium salt MTT for the last 4 h of incubation. After incubation, the scaffolds were briefly rinsed in PBS, blotted, and allowed to dry. Images of the scaffolds were obtained using a stereomicroscope fitted with a digital camera to qualitatively assess the distribution of insoluble purple formazan, a product of mitochondrial reduction of MTT by viable cells.

3. Results and Discussion

3.1. Structural characteristics of bioactive glass scaffolds

Figure 2 shows optical images of 13-93 bioactive glass constructs, as-formed by the FEF technique (Figure 2a), and after sintering at 700°C (Figure 2b). The as-formed construct (approximately 36 mm × 30 mm × 6 mm thick) was obtained by extrusion of the paste through an orifice of diameter 580 μm. The diameter of the deposited filaments (~600 μm) was slightly larger than the diameter of the orifice due to expansion of the plastic paste upon extrusion. As shown, the width of the pores in the plane of the deposition was ~500 μm and the porosity of the as-formed FEF construct was ~75% (including the porosity of the glass filaments).

There was no measurable shrinkage of the FEF scaffold during the freeze drying step, and the shrinkage during the binder burnout step was small (linear shrinkage <3%). However, the construct shrank considerably during the sintering step, as a result of the densification of the network of fine glass particles. The linear shrinkage was ~28% in the plane of deposition, and ~20% in the thickness direction of the scaffold. The sintered scaffolds consisted of glass filaments with a thickness of ~300 μm, porosity of ~50%, and pore width (in the plane of the deposition) of 300 μm (Table II).

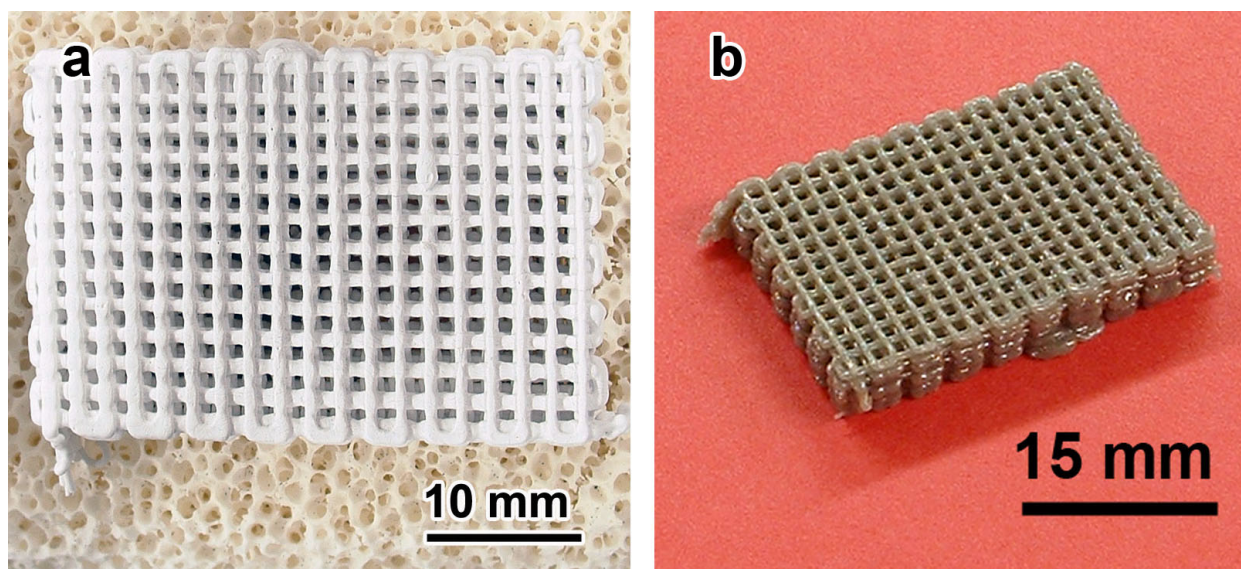


Figure 2. Optical images showing a bioactive glass construct (a) as-formed by the FEF technique, and (b) after binder burnout and sintering.

Table II. Structural characteristics of bioactive glass scaffolds as-formed by FEF and after sintering at 700°C.

Parameter	FEF scaffold	Sintered scaffold
Filament diameter (μm)	600	300
Porosity (%)	75*	50
Pore width (μm)	500	300

*Porosity including the porosity in the filaments before sintering

As Figure 2 shows, the FEF construct retained its shape and architecture during the post-processing steps (freeze drying, binder burnout; sintering). SEM images of fractured cross sections (Figure 3) showed that sintering resulted in almost complete densification of the glass phase, and the glass network contained only a few fine, isolated pores. Furthermore, there was good bonding between the adjacent layers of the sintered scaffold. These structural characteristics are desirable for enhancing the overall strength of the sintered scaffold. The ability to achieve nearly full density presumably resulted from the fine particle size of the

starting glass particles ($<3\ \mu\text{m}$), the homogeneous mixing of the particles and binder phase in the paste used in the extrusion, and high packing density of the glass particles in the paste.

Figure 3a shows that the pore width ($100\text{--}150\ \mu\text{m}$) in the thickness direction of the sintered scaffold was smaller than that in deposition plane ($\sim 300\ \mu\text{m}$). This smaller pore width in the thickness direction resulted presumably from deformation due to gravitational effects during the FEF step and particularly during the sintering step. In sintering, the reduction in the viscosity of the glass, necessary to achieve viscous flow densification of the glass phase and bonding between adjacent layers of the scaffold, also enhanced deformation of the glass by creep under the force of gravity.

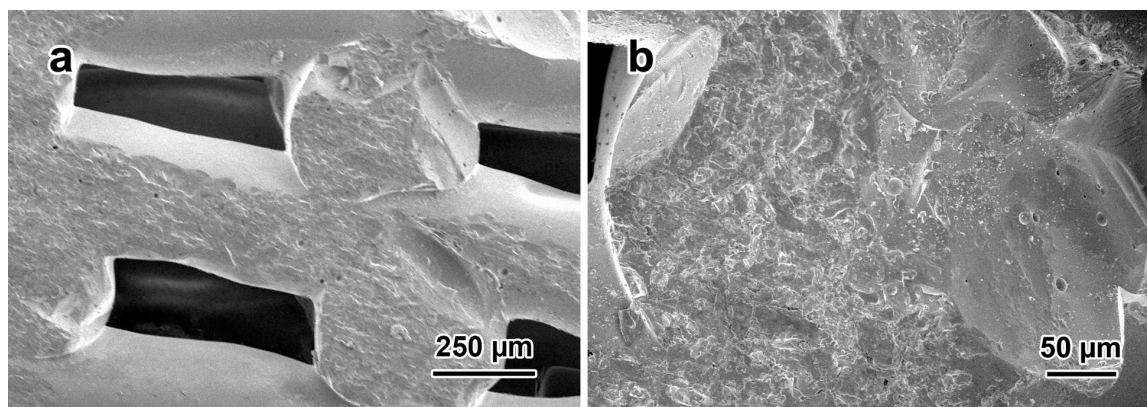


Figure 3. SEM images of the fractured cross section of a sintered bioactive glass scaffold showing (a) good bonding between adjacent layers of the scaffold, and (b) almost full densification of the glass phase. (The section was along the thickness direction of the scaffold.)

X-ray analysis of the sintered scaffolds did not show any diffraction peaks (Figure 4). Instead, the XRD pattern showed a broad band (centered at $\sim 30^\circ 2\theta$) characteristic of a glass. The ability to avoid crystallization of the bioactive glass during the scaffold fabrication process is beneficial for achieving high density of the glass network in the scaffold (and, hence for achieving high strength) and for maintaining the bioactive potential of the glass. Crystallization during sintering leads to a glass–ceramic material which is often difficult to densify. Furthermore,

while the glass–ceramic still retains the ability to form a hydroxyapatite surface layer, the rate of formation of the hydroxyapatite layer is markedly reduced.

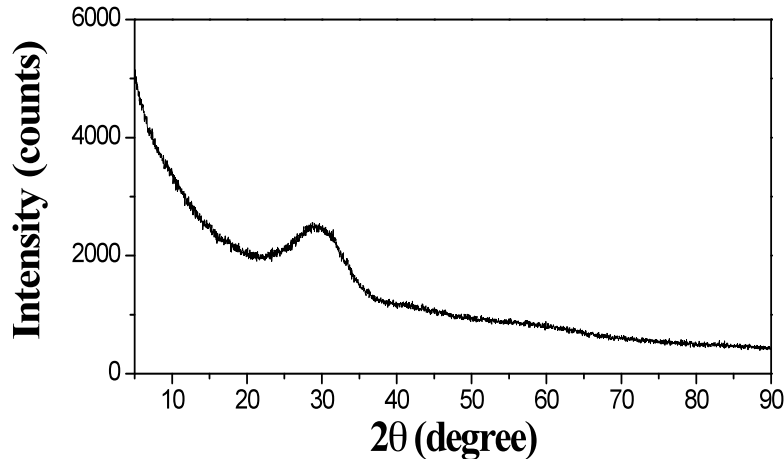


Figure 4. X-ray diffraction pattern of sintered bioactive glass scaffold, showing that the glass remained amorphous after the sintering step.

3.2. Mechanical response of sintered bioactive glass scaffolds

Figure 5a shows cube-shaped samples that were used in tests to measure the mechanical response of the sintered scaffolds in compression. The scaffolds showed a brittle response, typical of dense ceramics and glass (Figure 5b). The applied compressive stress increased almost linearly with the deformation until the sample failed in a catastrophic manner into several pieces. For the 6 samples tested, the compressive strength of the scaffold was 140 ± 70 MPa. This average strength is in the range of values reported for human cortical bone (120–180 MPa). The large standard deviation in the compressive strength may result from sample non-uniformity due to the small size of the samples tested and from macroscopic flaws arising from the FEF process. Since the linear dimension of the samples was 5 mm, variable in the sample uniformity can have a marked effect on the mechanical properties. The elastic modulus of the samples, determined from the slope of the stress vs. strain data, was 5–6 GPa, which is lower than the elastic modulus

of cortical bone (10–20 GPa).

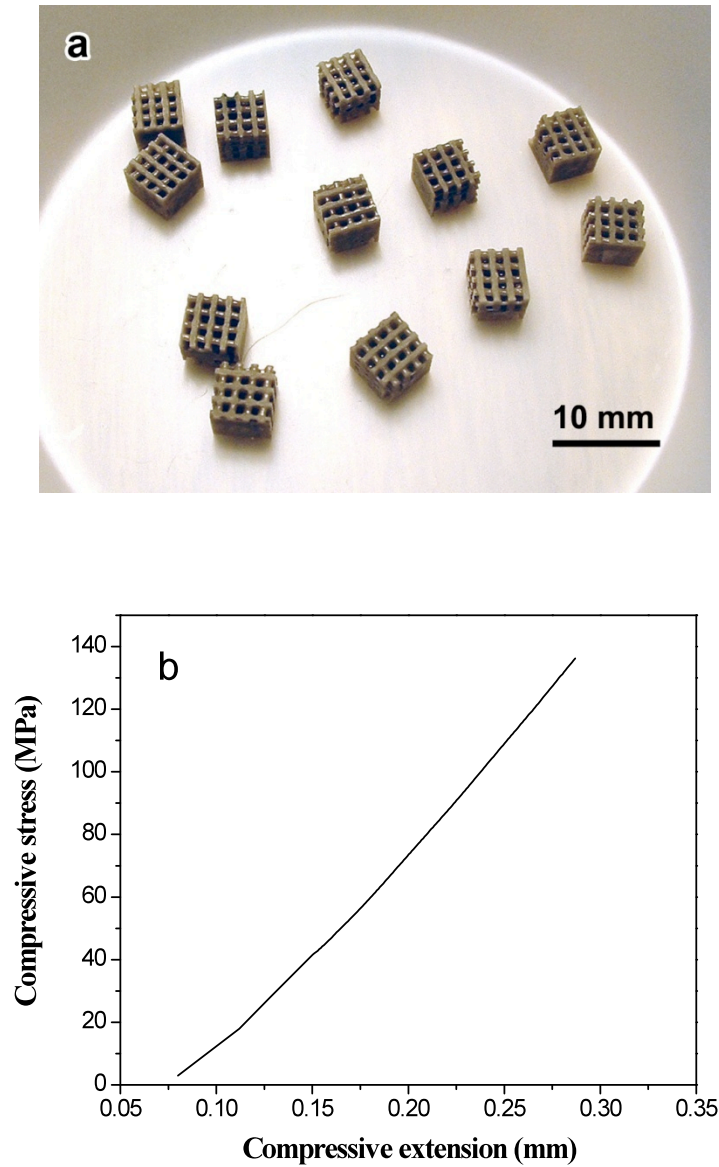


Figure 5. (a) Cube-shaped samples (5 mm in length) used in mechanical testing; (b) mechanical response (applied stress vs. deformation) of a sample in compression.

Table III shows a comparison of the compressive strengths of biodegradable polymer, bioactive glass, and hydroxyapatite scaffolds prepared by various methods [30]. The values shown in Table III are not meant to be exhaustive. Instead, they show the results of selected studies for various biomaterials and scaffold fabrication techniques. Although the compressive

strength in the present study showed a large standard deviation, the lowest strength (60 MPa) is still far higher than the strengths of biodegradable polymer scaffolds, as well as bioactive glass and hydroxyapatite scaffolds prepared by more conventional methods.

Table III. Summary of pore characteristics and compressive strength of scaffolds fabricated by a variety of methods [30].

Technique	Material	Open Porosity (%)	Pore Size or Dimension (μm)	Compressive Strength (MPa)
Freeze casting	HA	47-52	5-30	12-18
	HA	50-65	80-110	7.5-20
	HA	40-65	20	40-145
TIPS	PLLA/HA(50:50)	90	50-200	0.4
	PLGA	93-94	50-60	0.38-0.58
	PDLLA/Bioglass [®]	93.5-94		0.07-0.08
	PLGA	90-96	114-137	0.2-0.9
	HA/Collagen	95	200-500	0.03
Polymer sponge	HA	86	420-560	0.21
	Glass reinforced HA	85-97.5	420-560	0.01-0.175
	HA	70-77	200-400	0.55-5
	45S5 Bioglass [®]	89-92	510-720	0.27-0.42
	Ca ₂ MgSi ₂ O ₇	63-90	300-500	0.53-1.13
Gel casting	HA	76-80	20-1000	4.4-7.4
	HA	72-90	17-122	1.6-5.8
SFF	PCL	61	360 × 430 × 620	3.1
	HA	35	334 × 469	30
	HA	41	250-350	34
Slip casting	13-93 glass	40-45	100-300	21-23
	HA	85	200-500	1.09-1.76
Gas foaming	PLGA	85-96	193-439	0.16-0.29
Fiber compacting	HA	13-33	500-500	6-13

3.3 Biocompatibility of sintered bioactive glass scaffolds

Photographic images of scaffolds seeded with MLO-5A cells, cultured for 2, 4, and 6 days, and treated with MTT during the last 4 h of incubation are shown in Figure 6. The purple pigment visible on the scaffold is an indication of viable cells, and is the result of mitochondrial reduction of MTT to an insoluble formazan product. The increase in the intensity of the purple color with time indicated the proliferation of viable, metabolically active cells on the scaffolds.

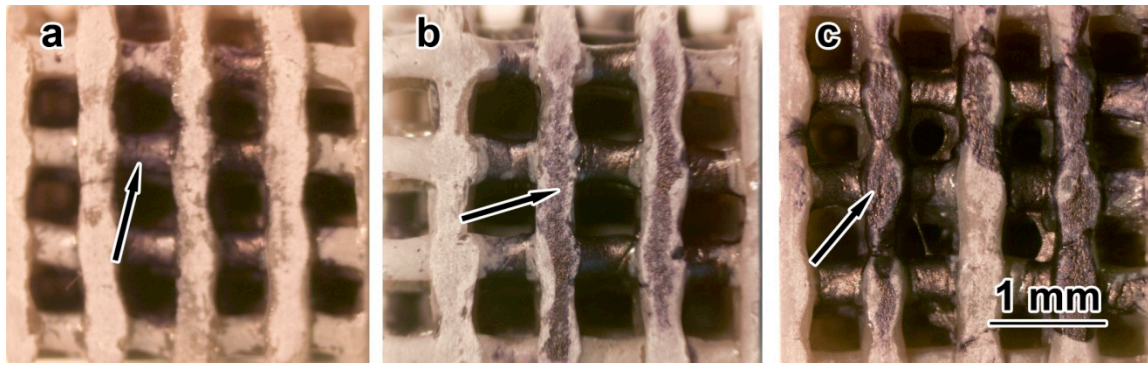


Figure 6. Optical images showing cell-seeded bioactive glass scaffolds treated with MTT after culture intervals of (a) 2 days; (b) 4 days, and (c) 6 days. The increase in intensity of the purple color (arrow) indicates the ability of the scaffolds to support cell proliferation.

The present work shows promising results for using the FEF technique in the fabrication of bioactive glass scaffolds for the repair and regeneration of load bearing bones. In addition to the benefit of other SFF methods in producing articles with predesigned external shape and internal architecture, the FEF was shown to produce porous 3D scaffolds with an almost fully dense glass network, which resulted in a compressive strength comparable to that of cortical bone.

4. Conclusions

The present results showed the feasibility of a freeze extrusion fabrication (FEF) technique for creating bioactive glass scaffolds with the requisite pore architecture and mechanical strength for potential application in the repair and regeneration of load-bearing bones. An extrudable paste was developed for the production of scaffolds with uniform shape and internal architecture. The scaffolds retained their external shape and internal architecture during the FEF process, as well as during the post-processing steps (freeze drying; binder removal; sintering). Sintered scaffolds of 13-93 glass with a porosity of ~50%, and interconnect pores of size $300 \times 300 \times 100\text{--}150 \mu\text{m}$, had a compressive strength of $140 \pm 70 \text{ MPa}$, comparable to the

strength of human cortical bone. These sintered scaffolds showed a brittle mechanical response in which the stress increased linearly with deformation until catastrophic failure. The scaffolds remained amorphous after sintering, and supported the proliferation of osteogenic MLO-A5 cells, showing their biocompatibility.

References

1. D.W. Hutmacher, "Scaffold design and fabrication technologies for engineering tissues – state of the art and future perspectives," *J. Biomater. Sci. Polymer Edn*, **12** [1] 107-12 (2001).
2. L.L. Hench, "Bioceramics," *J. Am. Ceram. Soc.* **81** 1705-28 (1998).
3. M.N. Rahaman, A. Yao, B.S. Bal J.P. Garino, and M.D. Ries, "Ceramics for prosthetic hip and knee joint replacement," *J. Am. Ceram. Soc.* **97** [7] 1965-88 (2007).
4. Z.Q. Chen, I.D. Thompson, A.R. Boccaini, "45S5 Bioglass-derived glass-ceramic scaffold for bone tissue engineering," *Biomaterials* **27** 2414-25 (2006).
5. Q. Fu, M.N. Rahaman, B.S. Bal, R.F. Brown, D.E. Day, "Mechanical and in vitro performance of 13-93 bioactive glass scaffolds prepared by a polymer foam replication technique," *Acta Biomaterialia* **4** 1854-64 (2008).
6. Q. Fu, M.N. Rahaman, B.S. Bal, W. Huang, D.E. Day, "Preparation and bioactive characteristics of a porous 13-93 glass, and fabrication into the articulating surface of a proximal tibia," *J. Biomedical Materials Research Part A*, **82** [1] 222-229 (2007)
7. S. C. Danforth, M. Agarwala, A. Bandyopadhyay, N. Langrana, V. R. Jamalabad, A. Safari, and R. Van Weeren, "Solid freeform fabrication methods," U.S. Patent No. US 5738817. (1998).
8. R. Wales and B. Walter, "Fast, precise, safe prototypes with FDM," *Proceedings of the Solid*

Freeform Fabrication Symposium, The University of Texas at Austin, Austin, TX, August 12–14, 1991; pp. 115-122.

9. S. Rangarajan, G. Qi, N. Venkataraman, A. Safari, and S. C. Danforth, “Powder processing, rheology, and mechanical properties of feedstock for fused deposition of Si_3N_4 ceramics,” *J. Am. Ceram. Soc.*, **83** [7] 1663-69 (2000).
10. G. M. Lous, I. A. Cornejo, T. F. McNlty, A. Safari, and S. C. Danforth, “Fabrication of piezoelectric ceramic/polymer composite transducers using fused deposition of ceramics,” *J. Am. Ceram. Soc.*, **83** [1] 124-28 (2000).
11. Bandyopadhyay, R. K. Panda, V. F. Janas, M. K. Agarwala, S. C. Danforth, and A. Safari, “Processing of piezocomposites by fused deposition technique” *J. Am. Ceram. Soc.*, **80** [6] 1366-72 (1997).
12. K. Nutt, “Selective laser sintering as a rapid prototyping and manufacturing technique,” *Proceedings of the Solid Freeform Fabrication Symposium, The University of Texas at Austin, Austin, TX, August 12-14, 1991; pp. 131-137.*
13. J. P. Kruth, P. Mercelis, L. Froyen, and M. Rombouts, “Binding mechanisms in selective laser sintering and selective laser melting,” *Rapid Prototyping J.*, **11** [1] 26-36 (2005).
14. E. M. Sachs, J. S. Haggerty, M. J. Cima, and P. A. Williams, “Three-dimensional printing techniques,” U. S. Patent No.5340656 (1994).
15. P. F. Jacobs, “Rapid Prototyping & Manufacturing: Fundamentals of Stereolithography,” 1st ed., Society of Manufacturing Engineers, Dearborn, MI, (1992).
16. J. III Cesarano, “A review of robocasting technology,” *Solid Freeform and Additive Fabrication: A Materials Research Society Symposium; Boston, MA, 1999; pp.133-139.*

17. T. S. Huang, M. S. Mason, X. Y. Zhao, G. E. Hilmas, and M. C. Leu, "Aqueous based freeze-form extrusion fabrication of alumina components," *Rapid Prototyping Journal* **15** [2] 88-95 (2009).
18. T.S. Huang, M.S. Mason, X. Zhao, G.E. Hilmas, and M.C. Leu, "Aqueous-based freeze-form extrusion fabrication of alumina components," *Rapid Prototyping J.* **15** [2] 88-95 (2009).
19. J. W. Wang, L.L. Shaw, A. Xu, T.B. Cameron, "Solid freeform fabrication of artificial human teeth," *Proceedings of the Solid Freeform Fabrication Symposium, The University of Texas at Austin, Austin Texas*, pp. 816-825. (2004).
20. J.G. Dellinger, J. Cesaraano III, F.D. Jamison, "Robotic deposition of model hydroxyapatite scaffolds with multiple architectures and multiscale porosity for bone tissue engineering," *J Biome Mater Res A*; **82A** 383-94(2007).
21. C.Y. Lin, T. Wirt, F.Lamarca, S.J. Hollister' "Structural and mechanical evaluations of a topology optimized titanium interbody fusion cage fabricated by selective laser melting process," *J Biomed Mater Res A* **83A** 272-9 (2007).
22. S. Foppiano, S.J. Marshall, G.W. Mashall, E. Saiz, A.P. Tomsia, "The influence of novel bioactive glasses on in vitro osteoblast behavior," *J. Biomed Mater Res A* **71A** 242-9 (2004).
23. T-M.G. Chu, D.G. Orton, S.J. Hollister, S.E. Feinberg, J.W. Halloran, "Mechanical and in vivo performance of hydroxyapatite implants with controlled architectures," *Biomaterials* **23** [5] 1283-93 (2002).
24. S.J. Hollister, R.D. Maddox, and J.M. Taboas, "Optimal design and fabrication of scaffolds to mimic tissue properties and satisfy biological constraints," *Biomaterials* **23** [20] 4095-103 (2002).
25. D.W. Hutmacher, M. Sttiger and M.V. Risbud, "Scaffold-based tissue engineering: rationale

- for computer-aided design and solid free-form fabrication systems,” *Trends in Biotechnology* **22** [7] 354-62 (2004).
26. J.M. Taboas, R.D. Maddox, P.H. Krebsbach, and S.J. Hollister, “Indirect solid free form fabrication of local and global porous, biomimetic and composite 3D polymer-ceramic scaffolds,” *Biomaterials* **24** [1] 181-94 (2003).
27. J. Franco, P. Hunger, M.E. Launey, A.P. Tomsia, E. Saiz, “Direct write assembly of calcium phosphate scaffolds using a water-based hydrogel,” *Acta Biomaterialia* **6** 218-28 (2010).
28. Y.J. Seol, J.Y. Kim, E.K. Park, S.Y. Kim, D.W. Cho, “Fabrication of a hydroxyl apatite scaffold for bone tissue regeneration using microstereolithography and molding technology,” *Microelectronic Engineering* **86** 1443-46 (2009).
29. R.F. Brown, D.E. Day, T.E. Day, S. Jung, M.N. Rahaman, Q. Fu, “Growth and differentiation of osteoblastic cell on 13-93 bioactive glass fibers and scaffolds,” *Acta Biomaterialia* **4** 387-96 (2008).
30. Q. Fu, M.N. Rahaman, F. Dogan, B.S. Bal, “Freeze casting of porous hydroxyapatite scaffolds. II. sintering, microstructure, and mechanical behavior,” *J. Biomed. Mater. Res. Part B: Applied Biomaterials*, **86B** 514-22 (2008).